Accepted Article

Authors: Laura Libero, Lara Ribeiro, L Granone, M Churio, Josiane Souza, Valmor Mastelaro, Juan Andres, Elson Longo, Lucia Mascaro, and Marcelo Assis

Introducing Structural Diversity: Fe$_2$(MoO$_4$)$_3$ Immobilized in Chitosan Films as an Efficient Catalyst for the Selective Oxidation of Sulfides to Sulfones

Laura O. Libero[a], Lara K. Ribeiro[a,b], Luis I. Granone[c], Maria S. Churio[c], Josiane C. Souza[a], Valmor R. Mastelaro[d], Juan Andrés[b], Elson Longo[a], Lucia H. Mascaro*[a] and Marcelo Assis*[b]

[a] L. O. Libero, Dr. L. K. Ribeiro, Dr. J. C. Souza, Prof. Dr. E. Longo, Prof. Dr. L. H. Mascaro
Center for Development of Functional Materials (CDMF)
Federal University of São Carlos (UFSCar)
Washington Luis Highway, km 235,13565-905, São Carlos, Brazil
E-mail: lmascaro@ufscar.br; http://lattes.cnpq.br/9130022476352844

[b] Dr. L. K. Ribeiro, Prof. Dr. J. Andrés, Prof. Dr. M. Assis
Department of Analytical and Physical Chemistry
Jaume I University
Vicent Sos Baynat Avenue, 12071, Castellón de la Plana, Spain
E-mail: marcelostassis@gmail.com; http://lattes.cnpq.br/3449316915846364

[c] Dr. L. I. Granone, Prof. Dr. M. S. Churio
Department of Chemistry and Biochemistry, Faculty of Exact and Natural Sciences, Institute of Physical Research of Mar del Plata (IFIMAR), CONICET
National University of Mar del Plata
AYL Mar del Plata AR, 3350 Deán Funes 3350, B7602AYL Mar del Plata, Argentina

[d] Prof. Dr. V. R. Mastelaro
São Carlos Institute of Physics
University of São Paulo (USP)
400 Trabalhador São Carlense Avenue, 13566-590, São Carlos, Brazil

Supporting information for this article is given via a link at the end of the document.

Abstract: This work reports how the immobilization of Fe$_2$(MoO4)$_3$ in chitosan films affects the oxidation reaction of sulfide derivatives to sulfates in the dark, resulting in good yields and excellent selectivity. As demonstrated, a variety of substituted sulfides were tolerated even in the presence of oxidative-sensitive functional groups, leading to a regioselective application of the catalyst under mild reaction conditions and guaranteeing its reuse for at least 6 cycles without losing its catalytic performance. Specifically, films containing 1 mg of Fe$_2$(MoO$_4$)$_3$ per ml of chitosan showed a yield and selectivity of 99%. The key success of the selective oxidation was associated with the presence of the hydroxyl radical, •OH, and the Fe^{3+}/Fe^{2+} Fenton-like process. As a proof of concept, the selective oxidation of sulfides to the corresponding sulfones was performed to demonstrate the synergistic effect between Fe$_2$(MoO$_4$)$_3$ and chitosan. This work offers a design strategy for efficient catalysts that may extend to other semiconductors and oxidation processes.

Introduction

The selective oxidation of sulfides to either sulfoxides or sulfones is one of the most important chemical processes in both chemistry and biology.[1] Sulfones are considered "chemical chameleons"[2] due to the possibility of modulating their reactivity through reaction conditions. For this reason, they have been commonly used as valuable synthetic intermediates in the production of new drugs, agrochemicals, and so on.[3] Traditionally, their synthesis is carried out at high temperatures using a catalyst to activate the oxidant.[4] Several catalysts can be used in this process, e.g., transition metal salts,[5] metal complexes,[6] metal-organic frameworks,[7] covalent organic frameworks,[8] polyoxometalates,[9] carbon-based materials[10] and semiconductor oxides.[11]

Metal oxides as inorganic semiconductors have drawn considerable attention because of their distinguished catalytic performance for the selective oxidation of sulfones. In this context, WO$_3$ has been employed for the photocatalytic oxidative desulfurization of organic sulfur-containing pollutants.[12] However, the severe recombination of electron–hole pairs in WO$_3$ leads to a low-efficiency photocatalytic reactions, making extensive application impossible. Zhao et al. studied the selective aerobic oxidation of sulfides to sulfoxides in water under blue light irradiation over Bi$_4$O$_5$Br$_2$ and obtained high yields in a relatively short time.[13] The oxidation of thioanisole was also achieved under visible light by modified ZnO–Fe$_3$O$_4$–Au nanoparticles.[14] Despite these findings, there is still room for improvements since most of the existing procedures have drawbacks, e.g., high temperatures, extended reaction times, use of large amounts of promoters and organic solvents, and difficulties related to the catalyst separation and recycling. Thus, the minimization of these impacts through the use of cleaner oxidants under mild conditions to achieve high selectivity and stability becomes an important point to be considered in the development of new technologies based on new and efficient catalysts.

Our research group has focused on the development of strategies to circumvent the above-mentioned bottlenecks. Very recently, MWO$_4$ (M = Cd, Co, Cu, Mn, Ni, and Zn) and α-Ag$_2$WO$_4$ semiconductors were proved as efficient and selective catalysts for the oxidation of sulfides to sulfones in the dark.[15] Iron molybdates such as Fe$_2$(MoO$_4$)$_3$ and FeMoO$_4$ could be promising catalysts for this type of reaction since they have been successfully used for the oxidation of methanol to formaldehyde.[16] The basic principle of the use of iron molybdate as a semiconductor catalyst is the increased generation of reactive oxygen species (ROS), consequently

RESEARCH ARTICLE

opening unfavorable reaction paths. If stabilized and supported on a strong framework with low cost and reduced environmental impact, these catalysts can become more efficient for further applications.

Biopolymers and biomasses are a class of catalyst supports that has been attracting growing interest due to their numerous advantages over conventional supports. In particular, chitosan has recently gained increased prominence as a by-product residue of the seafood processing industry, mainly shells of crustaceans such as crabs, shrimps, prawns and krill. Second most abundant structural polysaccharide in the world, [17] this substance also has high versatility, which allows it to be used in its polymeric form or through its calcined carbon biomass residue. [18] Very recently, we presented a chitosan/α-Ag_2WO_4 composite generated by femtosecond laser irradiation as a highly efficient material to kill bacteria and inactivate SARS-CoV-2 by contact, showing the existing synergistic effect between chitosan and α-Ag_2WO_4. [19] We also developed new catalysts for the dehydrogenative coupling of silanes with alcohols through the immobilization of Ag and Cr nanoparticles on the surface of an N-doped carbon support derived from the burning of chitosan. [20] In this context, Zheng et al. used Pd nanoparticles immobilized in chitosan films for application in Suzuki coupling reactions. [21] When materials derived from chitosan were used as a support for new catalysts, this resulted in catalysts with good stability and easy recyclability. In this regard, the search for the enhanced activity of these catalysts with moderate energy barriers will open new avenues for achieving a variety of potential applications.

Motivated by previous studies on the suitability of $NiWO_4$ and α-Ag_2WO_4 for the selective catalytic reduction of sulfides,[22] the advantages of chitosan, [23] and the fact that an efficient method for selective sulfide oxidation still remains a challenge, in this work we aimed to investigate the immobilization of $Fe_2(MoO_4)_3$ particles in chitosan polymeric films, given the essential role of this substance in applications. The films were characterized by X-ray diffraction (XRD), Raman spectroscopy, Fourier transform infrared spectroscopy (FT-IR), diffuse reflectance (DRS), scanning electron microscopy (SEM), atomic force microscopy (AFM) and X-ray photoelectron spectroscopy (XPS). The reaction parameters, i.e., temperature, time, solvent, catalyst loading, and type and amount of oxidant, were optimized according to the highest selectivity for sulfones. The recyclability, stability and scalability of the reaction were evaluated as well. Furthermore, the mechanism of action of the composite was analyzed through scavenger experiments, radical probe mass spectrometry (RP-MS), and electron paramagnetic resonance (EPR) spectroscopy. The results obtained show that this catalyst is extremely efficient in the sulfide oxidation process, working under mild and easy scalability. The corresponding mechanism was elaborated to guide the design of this highly active catalyst.

Results and Discussion

Structure of catalysts

The structural order at long range of the samples was determined by XRD and is presented in Figure 1A. As it can be seen, the synthesis using the microwave method gave rise to $Fe_2(MoO_4)_3$ with a monoclinic lamellar structure and space group *P12$_1$/a1*, in accordance with card No. 10060 in the Inorganic Crystal Structure Database (ICSD). [24] This structure is formed by distorted tetrahedral clusters of [MoO_4] and distorted octahedral clusters of [FeO_6]. No secondary phase was observed in this material, confirming the high efficiency of the synthesis process. In addition, the narrow and well-defined peaks point to a high crystallinity of the sample. For the pure chitosan films, the peak located at 11.6° can be attributed to the anhydrous semicrystalline polymer and is characteristic of chitosan films prepared by the polysaccharide dissolution in acetic acid and subsequent drying at low temperatures. [25] For the composite materials with $Fe_2(MoO_4)_3$ immobilization in chitosan, it is possible to observe a peak referring to the semi-crystalline polymer located at 22.9°, indicating that no changes occurred in the crystalline structure of $Fe_2(MoO_4)_3$ and chitosan after the composite formation. Defined through thermogravimetric tests, the content (% mg/mg) of $Fe_2(MoO_4)_3$ used in the composites was 12, 21 and 35% of $Fe_2(MoO_4)_3$ for the Fe100, Fe200 and Fe400 catalysts, respectively (Figure S1).
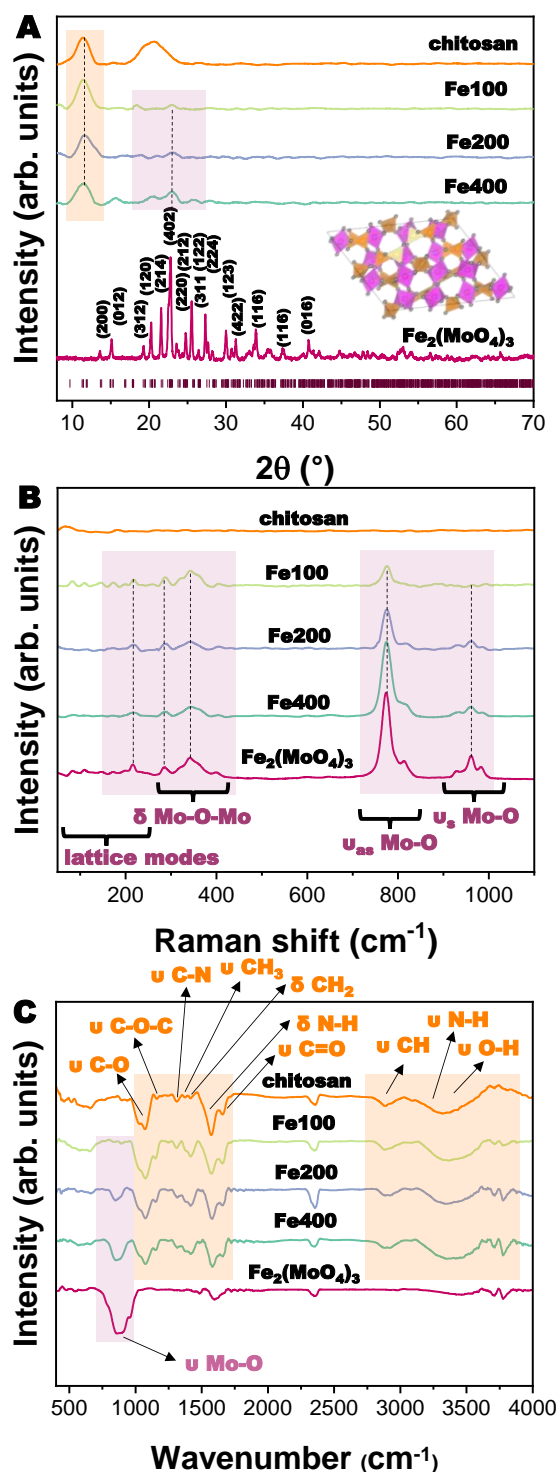
RESEARCH ARTICLE

Figure 1. A) XRD, B) Raman and C) FTIR spectra of the samples

Raman spectroscopy was performed to analyze the order at short range of the samples (Figure 1B). As observed, $Fe_2(MoO_4)_3$ exhibits three characteristic modes at 985, 963 and 928 cm^{-1} related to the symmetric stretching of Mo-O bonds of the [MoO$_4$] clusters, [26] whereas the modes located at 814 and 773 cm^{-1} refer to the anti-symmetric stretching of these bonds. [27] The three modes located between 282-400 cm^{-1} are assigned to the bending modes of the O-Mo-O angle, while those below 280 cm^{-1} correspond to the $Fe_2(MoO_4)_3$ lattice modes. [28] As expected, for being a semicrystalline polymer the pure chitosan does not have active Raman modes. However, it is possible to note the characteristic Raman modes of $Fe_2(MoO_4)_3$ in the composite samples, evidencing that the crystalline lattice of $Fe_2(MoO_4)_3$ was maintained. Furthermore, a reduction in the intensity and definition of the Raman modes is observed as a function of the concentration of $Fe_2(MoO_4)_3$ in the composite samples, following the order

3

RESEARCH ARTICLE

Fe400>Fe200>Fe100. This result is linked to the reduction in the amount of $Fe_2(MoO_4)_3$ within the catalyst, and also to the interaction of surface clusters of $Fe_2(MoO_4)_3$ particles with chitosan monomers, increasing the short-range disorder of the composite samples.

The FTIR spectra of the samples are shown in Figure 1C. The broad band between 700 and 900 cm^{-1} is attributed to the stretching of Mo-O bonds of the [MoO$_4$] clusters. [29] It is interesting to note that, as in Raman spectroscopy, the bands related to $Fe_2(MoO_4)_3$ vary in intensity as function of the added amounts. The broad band located between 3000 and 3700 cm^{-1} corresponds to the stretching of N-H and O-H bonds and to the presence of intramolecular hydrogen bonds, [30] while that located at 2880 cm^{-1} can be associated to the symmetrical and asymmetrical stretching of C-H bonds typical of polysaccharides. [31] The presence of N-acetylated groups can be confirmed by the bands at 1667, 1577 and 1308 cm^{-1} referring to the C=O stretching of amide I, the N-H bending of amide II and the C-N stretching of amide III, respectively. [32] The band located at 1577 cm^{-1} is related to the N-H bending of the primary amine, while those at 1403 and 1370 cm^{-1} refer to the bending of CH$_2$ and the symmetric stretching of CH$_3$, respectively. [33] Lastly, at 1157 cm^{-1} and between 1020-1070 cm^{-1}, it is possible to observe the C-O-C bridge asymmetric stretching and C-O stretching bands, respectively. [34] As observed in the results of Raman spectroscopy, there is a loss of definition of the bands related to the vibrations of the polymer, especially those related to the amide groups of the chitosan polymer. Such result may be related to the interaction of these functional groups with the surface clusters of $Fe_2(MoO_4)_3$.

According to the XPS survey spectra (Figure S2A, see Supplementary Information), the chitosan film exhibits peaks related to the elements C $1s$, O $1s$ and N $1s$, demonstrating the high purity of the samples. For the Fe100 film, in addition to the elements related to chitosan, it is also possible to observe Fe $2p$ and Mo $3d$ peaks, proving the presence of $Fe_2(MoO_4)_3$ in the obtained composites. In order to further explore this behavior, high-resolution analyses of the components obtained were carried out (Figures S2B-L). The high-resolution results for the N $1s$ spectra of chitosan revealed a peak at 400 eV decomposed into two components: a peak at 398.5 eV and another at 400.2 eV, corresponding to amine and amide groups, respectively. The atomic proportions of these peaks were 76 and 24%, respectively, approaching the deacetylation degree value of 75% of the chitosan used in the synthesis. [35] In the Fe100 sample, the high-resolution N $1s$ spectra did not show significant changes in the atomic proportions. The high-resolution C $1s$ spectra of chitosan and Fe100 were fitted into four components at 283, 284, at 285, and 287 eV, corresponding to the hydrocarbon (C–C), amide/amine (C–N/C=N), acetal (O–C–O) and C=O bonds, respectively, [36] while the O $1s$ spectra were fitted into three components at 530, 531 and 532 eV, referring to the N–C=O, C–O–C and –C–OH, respectively. [37] In the Fe100 sample, there was an increase in the number of C–O–C bonds and a decrease in the number of –C–OH and N–C=O bonds. These results corroborate those previously observed by Raman and FTIR spectroscopy, proving that there is interaction between chitosan and $Fe_2(MoO_4)_3$ particles, especially by the functional groups of chitosan rich in electrons. Additionally, at 530 eV the component was associated with the presence of O–Fe/Mo bonds of $Fe_2(MoO_4)_3$ and the sample also experienced a decrease in –C–OH bonds. Thus, it can be inferred that the addition of $Fe_2(MoO_4)_3$ to chitosan promoted a loss of surface hydroxyls in the sample.

The Fe100 sample also exhibited two predominant peaks with binding energies of 724 and 710 eV, which were attributed to Fe $2p_{1/2}$ and Fe $2p_{3/2}$, respectively. The Fe $2p_{3/2}$ spectra were fitted with peaks located at 714 (Fe^{2+}) and 711 eV (Fe^{3+}), whist the Fe $2p_{1/2}$ spectra were fitted with peaks located at 724 (Fe^{2+}) and 726 eV (Fe^{3+}). In contrast, the high resolution results for Mo $3d$ revealed the predominance of two peaks with binding energies of 231 and 234 eV, which were assigned to Mo $3d_{5/2}$ and Mo $3d_{3/2}$, respectively, due to the Mo^{5+}-Mo^{6+} process and molybdenum d-d transitions. The Fe100 sample exhibited unchanged characteristic peaks of Mo $3d$, indicating that the presence of chitosan did not alter the state of Mo^{6+} in $Fe_2(MoO_4)_3$. On the other hand, the Fe100 sample showed differences in the deconvolution of the $2p$ orbital, demonstrating a decrease in the percentage of Fe^{3+} and an increase in Fe^{2+} in relation to the pure $Fe_2(MoO_4)_3$, possibly because of the existence of charge transfers in chitosan that act on the changes perceived in the XPS for Fe $2p$. The deconvolution percentage of the high-resolution XPS curves of the samples is listed in Table S1.

The SEM images of the samples are shown in Figure 2. As it can be seen, unlike the composite samples the pure chitosan film does not have particles on its surface, demonstrating that the addition of $Fe_2(MoO_4)_3$ alters the surface of the composites. To corroborate these results, AFM analyses were performed. The obtained results reveal a certain homogeneity of the films with varying the concentrations of $Fe_2(MoO_4)_3$, leading to an increase in film roughness according to the order chitosan<Fe400<Fe200< Fe100. This indicates that the film roughness is inversely proportional to the amount of $Fe_2(MoO_4)_3$ because of the greater agglomeration of particles within chitosan with lower concentrations of $Fe_2(MoO_4)_3$. The roughness results can be seen in Table S2.
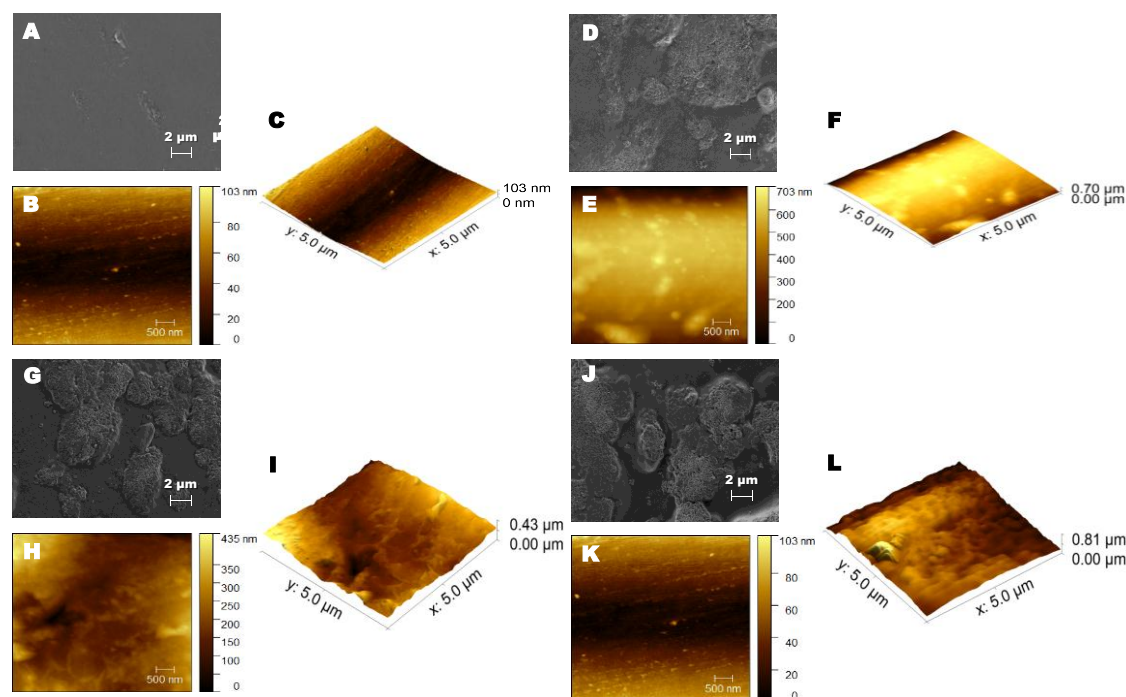
RESEARCH ARTICLE

Figure 2. SEM and AFM images of A-C) chitosan, D-F) Fe100, G-I) Fe200, and J-L) Fe400 samples

Catalyst performance

In this work, methylphenyl sulfide (thioanisole) was selected as a model molecule for the optimization of the catalytic conditions of the process. The oxidation of thioanisole can give rise to two distinct products: methylphenyl sulfoxide and methylphenyl sulfone, with the former being the intermediate reaction of sulfone (Figure 3A). According to Cervantes-Macias et al., since the oxidation of sulfoxide to sulfone is a process that involves a high activation energy (E_a = 90 Kcal/mol), it becomes a challenge to obtain sulfones in a selective and efficient way.[38] Among the catalytic conditions to be optimized, catalyst composition, temperature, time, type of solvent and oxidant, amount of oxidant and catalyst loading were taken into account. As a starting point, 0.1 mmol of thioanisole, 1.2 mmol of H_2O_2, 10 mg of catalyst and 2 mL of acetonitrile were used. According to Figure 3B, when used with total selectivity for sulfones the Fe100 catalyst reached conversions greater than 99% at a reaction time of 30 min and a temperature of 50°C. At shorter reaction times (15 min, Figure S3A), high conversions were still obtained (>92%), but with selectivity below 71%. Although longer times were also used, the results were similar to those obtained at 30 min (Figure S3B).

Temperature was an important parameter to obtain higher conversion values. At 30 °C (Figure S3C), low conversions and selectivity for sulfones were observed for all catalysts. Between 50°C (Figure 4B) and 70°C (Figure S3D), no significant differences were found when comparing the catalysts used. Thus, to proceed with the optimization conditions, the reaction time was set at 30 min and the temperature at 50°C. Fe100 (1 mg $Fe_2(MoO_4)_3$ / 1 mL chitosan) was used as a model catalyst as it achieved results similar to those of the other catalysts with higher $Fe_2(MoO_4)_3$ content (Fe200 and Fe400). Smaller proportions of $Fe_2(MoO_4)_3$ were also tested (0.5 mg $Fe_2(MoO_4)_3$ / 1 mL chitosan), but the conversion and selectivity values obtained were lower than 80%. Therefore, it can be concluded that the oxidation model employed is dependent on time, temperature and amount of $Fe_2(MoO_4)_3$ immobilized in chitosan. Control experiments with H_2O_2 showed that the conversion rate of chitosan used as a catalyst and H_2O_2 alone were similar (<45%), with a selectivity for sulfone of ~30%.
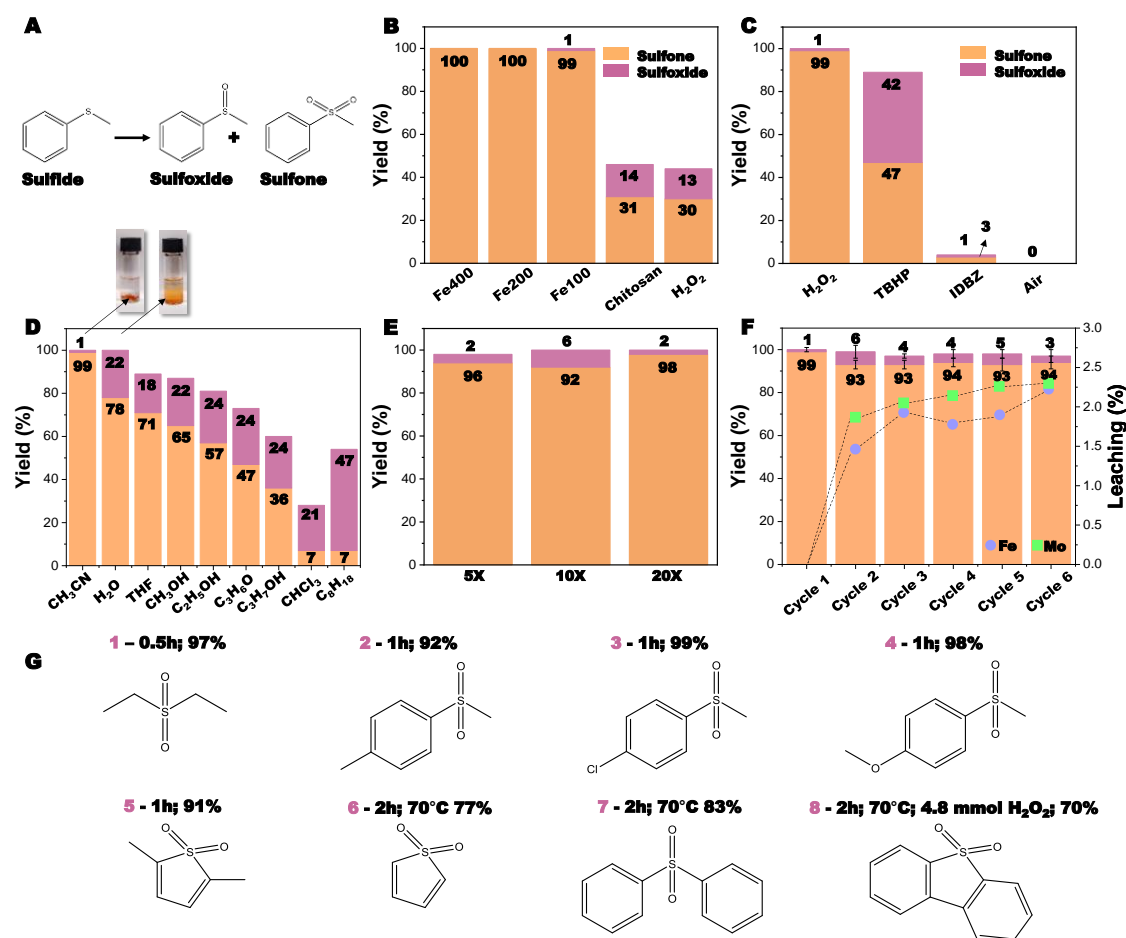
RESEARCH ARTICLE

Figure 3. A) Reaction scheme. B) Reaction performed at 50°C and 30 min, using 2 mL of acetonitrile, 10 mg of catalyst and 1.2 mmol of H_2O_2; C) reaction performed at 50°C and 30 min, using 2 mL of acetonitrile, 10 mg of catalyst and 1.2 mmol of different oxidants; D) reaction performed at 50°C and 30 min, using 2 mL of solvent, 10 mg of catalyst and 1.2 mmol of H_2O_2; E) reaction scale-up; F) catalytic recycles and leaching of Fe and Mo per recycle (using acetonitrile as solvent); and G) catalytic scope.

The influence of different oxidants was also evaluated (Figure 3C). As it can be seen, although the use of tertbutyl hydroperoxide (TBHP) resulted in a high conversion value, the selectivity for sulfones was low (~47%). Iodobenzene (IDBZ) and atmospheric air bubbled in solution were used as possible oxidants as well, however, no significant conversion value was observed. Since H_2O_2 was selected as the best oxidant, smaller amounts of H_2O_2 were used in the oxidation reaction, but the conversion and selectivity values dropped significantly (Figure S4A). The catalyst loading was another parameter analyzed (Figure S4B). According to the tests, the best conversion was obtained with 10 mg of catalyst.

In relation to the solvent, alcohols, acetone, THF, chloroform and n-octane achieved much smaller conversion and selectivity values (Figure 4D). In contrast, when water was employed as a solvent, a conversion value similar to that of acetonitrile was obtained, with a selectivity for sulfone of 78%. since the value of water is much lower than that of acetonitrile, this result is extremely important when considering the final value of the process. However, at the end of the catalytic cycle using water as a solvent, the catalyst dissolved in solution, making its recovery and recycling impossible. This is because chitosan can absorb water by dissolving in the reaction medium. [39] Using chloroform and n-octane as solvents, the selectivity for sulfoxide was greater, so other conversion times were tested in order to selectively obtain both oxidation products (Figure S5A-B). It is observed that using chloroform as solvent with longer reaction times (1h and 2h), the selectivity for the sulfoxide increases (33%), but the total conversion is still very low (35%). When n-octane is used as a solvent, increasing the reaction time to 2h, high selectivity for the sulfoxide is obtained (80%), with high conversion values (84%). This shows that by changing only the solvent, the same catalyst can be used to obtain both oxidation products.

Another point investigated was the scale-up of the oxidation process at 5, 10 and 20 times (Figure 3E). As observed, high conversion and selectivity values were obtained in all cases, evidencing the ease of the reaction scale-up. Catalyst recycling was analyzed in successive catalytic cycles using the same catalyst (Figure 3F). In 6 successive cycles the catalyst achieved conversion values above 97% and a selectivity for sulfone higher than 93%. This result demonstrates that the use of chitosan as a catalyst support facilitates the separation of the catalyst from the reaction medium, thus increasing its stability. Fe and Mo leaching was analyzed between catalytic cycles by ICP-OES, with a maximum leaching of 2.3% per cycle (Figure 3F). To verify that the catalytic process comes from the heterogeneous catalyst and not from the species leached in solutions, control tests with the ionic species in solution (Fe^{3+} and $(MoO_4)^{2-}$) were carried out, showing conversions very close to those of H_2O_2 (Figure S6). Tests with $Fe_2(MoO_4)_3$ in

RESEARCH ARTICLE

equimolar amounts in relation to the catalyst were also performed, resulting in a conversion of 80% and a selectivity for sulfone of 28%. This evidences the existing synergy between $Fe_2(MoO_4)_3$ and chitosan, which makes the composite catalysts more effective. As n-octane showed selectivity for sulfoxide, its catalytic recycle was also carried out, however low stability of the catalyst was observed in this solvent, showing low conversion and yield after the second recycle (Figure S7).

The catalytic scope was extended to substrates with other aromatic and aliphatic R_1-S-R_2 (R_1, R_2 = alkyl, aryl) sulfides and thiophene-derived sulfides (Figure 3G). Aliphatic thioethers were oxidized under the same conditions as those used for thioanisole, reaching a selectivity for sulfones above 97%, while 2,5-dimethylthioanisole (DMT) and thioanisole derivatives with p- substitutions were oxidized twice as long, resulting in a selectivity higher than 90%. Symmetrical aromatics, thiophene, and dibenzothiophene (DBT) required a higher temperature (70°C) and longer times to achieve a selectivity value above 70%. It is expected that other substrates based on sulfides need additional additives or reaction conditions different from the model used in this work for the oxidation reaction to occur due to their chemical characteristics.

Mechanism

A semiconductor is governed by electronic motion between its valence (VB) and conduction bands (CB), generating an electron density deficit in the VB and an accumulation of electron density in the CB. [40] This change in electronic density is spontaneous and can be amplified according to the absorption of electromagnetic radiation or electric field by the system, or due to an increase in temperature, for example. [41] This deficit or accumulation of electron density can interact with the surrounding environment, causing a cascade of chemical reactions. [42] It is important to mention that in our case the catalyst works in the dark – although the previous arguments are valid if enough energy is provided to obtain the corresponding ROS. H_2O_2 can interact directly with the regions with electron density deficit, giving rise to two hydroxyl radicals (•OH) that can actively participate in the oxidation of sulfides. [43] In addition, H_2O_2 can decompose into H_2O, which in turn interacts with the regions with deficit of electron density, forming an •OH and a proton (H^+), while the molecular oxygen (O_2) can interact with the accumulation of electron density, generating a superoxide radical (•O_2^-) and evolving into an oxygen singlet ($^1O_2$), or with an H^+, forming a hydroperoxyl radical (•O_2H). [44]

To investigate the oxidation mechanism, specific scavengers were used for the $^1O_2$ (ascorbic acid, AA), •O_2H (p-benzoquinone, BQ) and •OH (potassium acid biphthalate, KABP) species, as well as for the electron density deficit, i.e., holes, h^+ (ammonium oxalate, AO), and the electron density accumulation, i.e., e^- (silver nitrate, SN) (Figure 4A). [45] A significant reduction in the conversion rate was not observed when scavengers of the $^1O_2$ and •O_2H species were used, evidencing that these species were not involved in the sulfide oxidation mechanism. However, when KABP, AO and SN were added, a sharp decrease in the conversion and selectivity of the oxidation process was observed, indicating that the •OH, h^+, and e^- species were directly involved in the oxidation process. However, as previously noted by Bao et al., the accuracy of the scavenger experiments for quantitative analysis is still very poor since the inhibition effect of these substances on the catalytic reaction is not only related to their antioxidant capacity, but also to the process of radical chain reaction. [46]
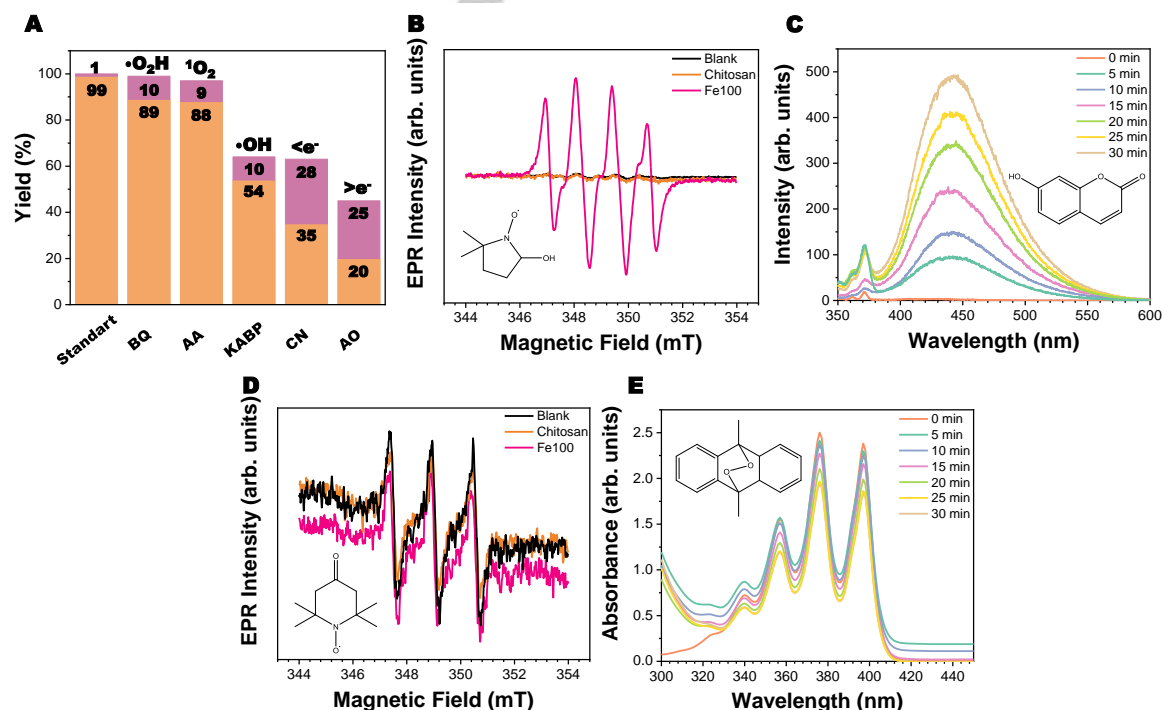

Figure 4. A) Reaction performed at 50°C and 30 min, using 2 mL of acetonitrile, 10 mg of catalyst and 1.2 mmol of H_2O_2 in the presence of different species of scavengers; B) detection of •OH by EPR using DMPO; C) fluorescence monitoring of coumarin oxidation by •OH; D) detection of $^1O_2$ by EPR using 4-oxo-TMP; and E) UV-Vis monitoring of DMA oxidation by $^1O_2$

The production of •OH and $^1O_2$ was further investigated by EPR and spectroscopic probes. The EPR spectra of the samples in Figure 4B indicate that the •OH was captured by DMPO, forming the DMPO-OH adduct only when Fe100 was used in association with H_2O_2.

7

RESEARCH ARTICLE

[47] The same was observed for the hydroxylation of coumarin (Figure 4C): the hydroxylated product of coumarin (7-hydroxycoumarin) fluoresced when excited at 332 nm, [48] showing that •OH radicals were generated in greater quantity when an association was made between the catalyst and H_2O_2 (Figure S8A-B). The production of •OH was also found to be time-dependent, suggesting that the decomposition of H_2O_2 and H_2O into •OH did not occur immediately.

The presence of $^1O_2$ was analyzed by EPR using 4-oxo-TMP to capture $^1O_2$ (Figure 4D). [49] Unlike the changes caused by the presence of •OH, no significant differences were observed among the blank (H_2O_2), the chitosan film and the Fe100 catalyst. This shows that if $^1O_2$ was indeed present, its production was very small. To verify this result, the presence of $^1O_2$ was determined using 9,10-dimethylanthracene (DMA), which reacts specifically with $^1O_2$ to form a stable endoperoxide, resulting in a decreased DMA absorption (Figure 4E). [50] As expected, no significant decrease in DMA absorption was observed for the catalyst associated with H_2O_2 or other separate species (Figure S8C-D), corroborating the EPR results.

$Fe_2(MoO_4)_3$ is an Fe-based semiconductor that can generate undercoordination at $[FeO_6]$ distorted octahedral clusters and form distorted octahedral clusters of $[FeO_5.V_O^x]$ in the Kröger-Vink notation due to the presence of oxygen vacancies (V_O^x). This imbalance corresponds to the Fe^{3+}-Fe^{2+} redox able to provoke Fenton-like oxidative processes. [51] To verify whether Fenton-like processes were activated for the generation of radicals from H_2O_2, an XPS analysis was performed after catalysis to observe the surface amount of Fe^{2+} and Fe^{3+}. By analyzing the Fe 2p spectra of the Fe100 sample after the use of the catalyst in the oxidation of sulfides to sulfones, it was possible to note a considerable increase in the surface amount of Fe^{3+} from 33.32 to 80.94 (%), which strongly indicates the occurrence of a Fenton-like process and surface modifications in the catalyst (Figure S9).

The proposed mechanism of radical production can be seen in Figure 5A. Chitosan is a polymer that contains a positive surface charge that works as an electron donor, [52] injecting electronic density into $Fe_2(MoO_4)_3$, in addition to H_2O_2 and H_2O, which will donate an electron to $Fe_2(MoO_4)_3$, forming •OH. This excess electron density is excited from the VB to the CB (E_{gap} = 2.14 eV) and this promotion is facilitated by intrinsic semiconductor defects in the forbidden region of the band gap. The O_2 generated from the decomposition of H_2O_2 accepts the electronic density accumulated in the CB, generating an •O_2^- radical, which in turn quickly joins with H^+ to render an •O_2H radical. As previously noted, this •O_2H does not effectively participate in the oxidation process; it quickly joins with •OH to form H_2O and O_2 and once again close the redox processes. On the other hand, the surface sites of $[FeO_5.V_O^x]$ and $[FeO_6]$ end up interacting with H_2O_2. In particular, $[FeO_5.V_O^x]$ reacts with H_2O_2, forming an •OH and a hydroxyl anion (OH^-), while $[FeO_6]$ interacts with H_2O_2 to render an •O_2H and an H^+. The •O_2H then interacts with •OH, as in the semiconductor, whilst the OH^- interacts with H^+, forming H_2O. Since the •OH species are generated by the intrinsic electronic movement of the semiconductor or by the Fenton-like process, these radicals attack the sulfur atom of the sulfides, resulting in the formation of the corresponding sulfoxide with subsequent elimination of H_2O. The same process is repeated to generate sulfone (Figure 5B).
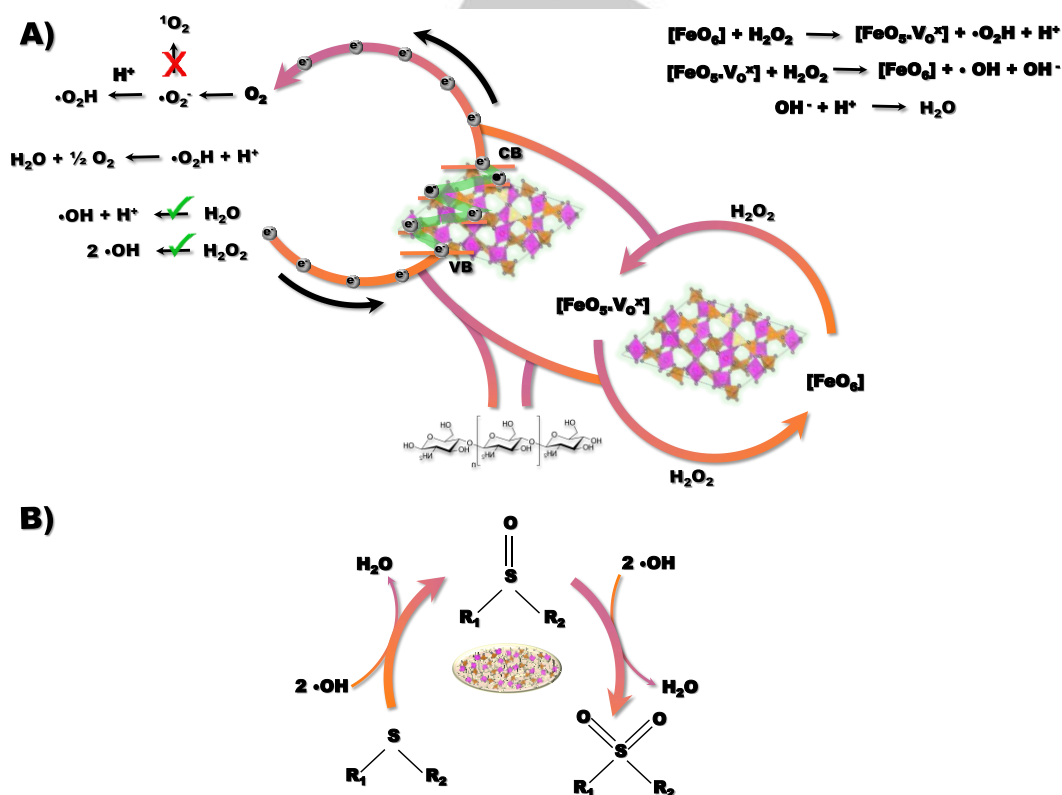

Figure 5. A) Activation mechanism of $Fe_2(MoO_4)_3$ immobilized in chitosan films and B) oxidation mechanism of sulfides by •OH radicals

Conclusions

RESEARCH ARTICLE

The main conclusions of the present work can be summarized as follows: (i) a practical catalytic system ($Fe_2(MoO_4)_3$ immobilized in chitosan films) for the oxidation of sulfides to sulfones was successfully developed; (ii) high yields of different kinds of sulfone products were obtained selectively in a relatively short time; (iii) the recyclability of the catalyst was considered good since it could be used several times without losing its performance; (iv) the films containing 1 mg of ($Fe_2(MoO_4)_3$ per ml of chitosan showed a yield and selectivity of 99%; and (v) from the results of scavenger experiments, radical probe mass spectrometry and EPR spectroscopy, a mechanism was proposed for an efficient oxidation reaction based on the presence of a hydroxyl radical, •OH, and the Fe^{3+}/Fe^{2+} Fenton-like process. In broad terms, this is a sustainable and efficient catalyst for the selective oxidation of sulfides to sulfones that could be applied using other semiconductors for the development of new catalytic technologies of oxidation processes with low environmental impact. This study will pave the way for the design of efficient catalysts and future success will be a result of further progress in multiple directions, including the study of their mechanism and preparation.

Experimental Section

Synthesis of $Fe_2(MoO_4)_3$: $Fe_2(MoO_4)_3$ was synthesized using the coprecipitation (CP) method followed by microwave hydrothermal treatment (MHT). First, 1×10^{-3} mol of $FeCl_2.4H_2O$ (98%, Aldrich) and 1×10^{-3} mol of $Na_2MoO_4.2H_2O$ (98%, Aldrich) were dissolved in two different beakers containing 50.0 mL of distilled water. After complete dissolution, the $FeCl_2.4H_2O$ solution was added to the $Na_2MoO_4.2H_2O$ solution under constant stirring at 30 °C, resulting in the formation of a dark red precipitate. This precipitate was transferred to a Teflon autoclave for MH treatment (2.45 GHz, maximum power of 800 W) operating at 160 °C for 32 min. The final precipitate was washed 5 times with distilled water and dried in a conventional oven at 60 °C for 12 h.

Preparation of catalysts: The chitosan solution was prepared by dissolving 2.0 g of chitosan (Infinitu Tech, medium molecular weight, 1250000>96.5%, degree of deacetylation of 75%) in 100 mL of aqueous solution of glacial acetic acid (P.A., Synth) at 1% (v/v) at room temperature. The solution was left under constant agitation for 24 h at room temperature for the complete dissolution of chitosan. The pH was adjusted to 4.8 through the slow addition of NaOH solution (0.1 M, 98%, Synth) and the resulting solution was filtered using a sintered plate filter no. 0. After this process, $Fe_2(MoO_4)_3$ was added to the solution of chitosan at concentrations of 1.0, 2.0 and 4.0 mg/mL and the mixture was placed in an ultrasound bath for 15 min. The solution was then transferred to a Petri dish and dried at 40 °C for 14 h for film formation. Lastly, these films were cut into discs of 0.5 cm in diameter.

Characterizations: The samples were characterized by XRD on a Rigaku X-Ray Diffractometer, model DMax2500PC. The equipment was operated at 40 kV and 60 mA using Cu-Kα radiation (λ = 1.5406 Å). A sweep rate of 0.02°/min was used in the range between 10 and 100°. The powder diffractograms were compared with the diffraction patterns according to the crystallographic sheets of the Inorganic Crystal Structure Database (ICSD). Raman spectroscopic data were obtained on an iHR550 spectrophotometer (Horiba Jobin-Yvon, Japan) equipped with a charge-coupled device detector and an argon ion laser (MellesGriot, USA) operating at 633 nm with a power of 200 mW. DRS analyses were carried out by the total diffuse reflectance method on a Varian Cary 5G spectrophotometer (Agilent, EUA) using an integrating sphere. Magnesium oxide (MgO) was adopted as the reference material for the DRS analysis. The FT-IR spectra were measured on a Jasco FT/IR-6200 (Japan) spectrophotometer operating in absorbance mode at room temperature in the range of 400-4000 cm^{-1}. SEM images were obtained using a Zeiss LEO 1550 electron microscope (Germany) with electrostatic emission source (FE-SEM) operating at 2 kV. XPS analyses were carried out on a Scientia Omicron ESCA spectrometer (Germany) using a monochromatic Al Kα X-ray source (1486.7 eV). Peak deconvolution was performed using a 70:30% Gaussian-Lorentzian line shape and a Shirley nonlinear sigmoid-type baseline. The binding energies of all elements were calibrated with reference to the C 1s peak at 284.8 eV. The samples were characterized using a Flex-AFM controlled by easyScan 2 software (Nanosurf, Switzerland) in contrast phase mode on an active vibration isolation table (model TS-150, Table Stable LTD®). The cantilever used for image acquisition was Silicon Tap190G (resonance frequency of 190 kHz, constant force of 48 N/m, Budget Sensors) at a setpoint of 50%. The chemical composition of the solutions during the catalytic cycles was estimated by inductively coupled plasma optical emission spectrometry (ICP OES) using an ICP OES iCAP 7000 (Thermo Fisher Scientific, USA).

Catalytic procedure: Catalytic tests were carried out in 4 mL vials under magnetic stirring at 700 rpm/min. The experimental procedure was performed by dispersing the catalyst in a solution with 0.1 mmol of sulfide substrate and 2 mL of solvent containing 15 μL of hexadecane (as an internal standard) followed by the addition of an oxidant to the reaction system. The parameters of catalyst loading (10, 7.5, 5 and 2.5 mg), solvent type (CH_3CN, H_2O, THF, CH_3OH, C_2H_5OH, C_3H_6O, C_3H_7OH and $CHCl_3$), oxidant type (H_2O_2 (35%,, 130v, Neon), TBHP (Aldrich), iodobenzene (98%, Aldrich) and air), oxidant volume (1.2 and 0.6 mmol), time (15, 30 and 60 min) and temperature (30, 50 and 70 °C) were optimized during the catalytic process. At the end of the catalysis, an aliquot was taken and diluted in 2 mL of ethyl acetate for analysis on a gas chromatograph (GC, Agilent 8860) provided with a flame-ionization detector (FID), using a non-polar (5%-phenyl)-methylpolysiloxane column (Agilent J&W HP-5). The analyses were performed in duplicate. Experiments with scavengers were carried out following the same procedure under optimized conditions, adding equimolar amounts of scavengers. To analyze the recyclability of the catalyst, the experiment was repeated using the same catalyst 6 times. The catalytic scope was performed using commercial sulfides and sulfones based on thioanisole and thiophene and identified the conversion by GC. The methods used in the GC for product detection can be found in the *Supporting Information*.

Identification of hydroxyl radical and singlet oxygen by EPR: For the detection of •OH, 5 μL of 5,5-dimethyl-1-pyrroline-N-oxide (DMPO, Aldrich) was mixed with 15.0 mg of the Fe100 film, 50 μL of 30 % H_2O_2, and 1.0 mL of acetonitrile. For the detection of $^1O_2$, 100 μL of a 0.115 mol L^{-1} solution of 2,2,6,6-tetramethyl-4-piperidone (4-oxo-TMP, Aldrich) in acetonitrile was mixed with 15.0 mg of the Fe100 film, 50 μL of 30 % H_2O_2, and 1.0 mL of acetonitrile. Blank experiments either without the Fe100 film or with 15.0 mg of the

RESEARCH ARTICLE

pure chitosan film were performed for both •OH and $^1O_2$ detection experiments. The EPR spectra of the samples were acquired at 293 K using a Bruker spectrometer, model ELEXSYS E500T (Germany) provided with an ER 4102ST rectangular resonator operating in the TE102 mode at a center frequency of 9.8 GHz (X-band). The following data acquisition parameters were used for the measurements: modulation frequency of 100.00 kHz, modulation amplitude of 0.200 mT, microwave power of 20.4 mW, central field of 349 mT, sweep width of 10 mT, and conversion time of 40.96 ms. A total of 1024 data points were collected per scan, and the resulting spectra were the average of 5 scans.

Identification of hydroxyl radical and singlet oxygen by spectroscopic probes: For the detection of •OH, 15 μL of a solution of coumarin (1000 ppm, Aldrich) was diluted in 10 mL of acetonitrile and placed in contact with the catalytic system. Aliquots were taken at 0, 5, 10, 15, 20, 25 and 30 min and analyzed using a spectrofluorophotometer (RF-5301 PC, Shimadzu, Japan) with excitation at 332 nm and emission monitored between 350 and 600 nm with slit = 5 nm. The detection of $^1O_2$ was performed using a solution containing 9,10-dimethylanthracene (2 mL, 1×10^{-4} M in acetonitrile, 98%, Aldrich). Aliquots were taken at 0, 5, 10, 15, 20, 25 and 30 min and analyzed using a V-660 spectrophotometer (Jasco, Japan), monitoring the absorption in the range of 300-450 nm.

Acknowledgements

Keywords: oxidation • heterogeneous catalysis • organic-inorganic hybrid composites • radical reactions • supported catalysts

[1] a) F. Rajabi, E. Vessally, R. Luque, L. Voskressensky, *Mol. Catal.* **2021**, *515*, 111931; b) S. Matavos-Aramyan, S. Soukhakian, M. H. Jazebizadeh, *Phosphorus Sulfur. Silicon Relat. Elem.* **2020**, *195*, 181; c) E. Voutyritsa, I. Triandafillidi, C. G. Kokotos, *Synthesis* **2017**, *49*, 917; d) S. Liang, K. Hofman, M. Friedrich, J. Keller, G. Manolikakes, *ChemSusChem*, **2021**, *14*, 4878.

[2] S. Liang, K. Hofman, M. Friedrich, J. Keller, G. Manolikakes, *ChemSusChem*, **2021**, *14*, 4878.

[3] a) X. Lang, W. R. Leow, J. Zhao, X. Chen, *Chem. Sci.* **2015**, *6*, 1075; b) A. Rajendran, T. Cui, H. Fan, Z. Yang, J. Feng, W. Li, *J. Mater. Chem. A* **2020**, *8*, 2246; c) V. Trombettoni, A. Franco, A. G. Sathicq, G. Len, G. P. Romanelli, L. Vaccaro, R. Luque, *ChemCatChem* **2019**, *11*, 2537; d) H. Hao, Z. Wang, J.-L. Shi, X. Li, X. Lang, *ChemCatChem* **2018**, *10*, 4545.

[4] a) H. Hao, Z. Wang, J.-L. Shi, X. Li, X. Lang, *ChemCatChem* **2018**, *10*, 4545; b) T. Zhang, J. Zhang, Z. Wang, J. Liu, G. Qian, D. Wang, X. Gong, *Fuel* **2021**, *305*, 121562.

[5] J. Legros, C. Bolm, *Chem. – A Eur. J.* **2005**, *11*, 1086.

[6] T. R. Amarante, P. Neves, F. A. Almeida Paz, A. C. Gomes, M. Pillinger, A. A. Valente, I. S. Gonçalves, *Catal. Sci. Technol.* **2021**, 11, 2214.

[7] F. Zhang, J. Zhang, B. Zhang, L. Zheng, X. Cheng, Q. Wan, B. Han, J. Zhang, *Green Chem.* **2020**, *22*, 5995.

[8] L. Liu, B. Zhang, X. Tan, D. Tan, X. Cheng, B. Han, J. Zhang, *Chem. Commun.* **2020**, *56*, 4567.

[9] D. Karimian, F. Zangi, *Catal. Commun.* **2021**, *152*, 106283.

[10] J. Li, Y. Chen, X. Yang, S. Gao, R. Cao, *J. Catal.* **2020**, *381*, 579.

[11] M. Kang, X. Wang, J. Zhang, Y. Lu, X. Chen, L. Yang, F. Wang, *J. Environ. Chem. Eng.* **2019**, *7*, 102809.

[12] a) V. A. Grinberg, V. V Emets, M. V Tsodikov, N. A. Mayorova, D. A. Maslov, *Prot. Met. Phys. Chem. Surf.* **2021**, *57*, 699; b) O. Samuel, M. H. D. Othman, R. Kamaludin, O. Sinsamphanh, H. Abdullah, M. H. Puteh, T. A. Kurniawan, *Ceram. Int.* **2022**, *48*, 5845; c) X. Xiao, H. Zhong, C. Zheng, M. Lu, X. Zuo, J. Nan, *Chem. Eng. J.* **2016**, *304*, 908; d) W. Zhu, F. Sun, R. Goei, Y. Zhou, *Appl. Catal. B Environ.* **2017**, *207*, 93.

[13] W. Zhao, C. Yang, J. Huang, X. Jin, Y. Deng, L. Wang, F. Su, H. Xie, P. K. Wong, L. Ye, *Green Chem.* **2020**, *22*, 4884.

[14] A. I. Cervantes-Macías, C. A. Huerta-Aguilar, T. Pandiyan, *J. Clust. Sci.* **2017**, *28*, 1897.

[15] M. Assis, A. F. Gouveia, L. K. Ribeiro, M. A. Ponce, M. S. Churio, O. N. Oliveira Jr., L. H. Mascaro, E. Longo, R. Llusar, E. Guillamon, *J. Andres, Appl. Catal. A Gen.* **2023**, *625*, 119038.

[16] a) A. P. V. Soares, M. F. Portela, A. Kiennemann, *Catal. Rev.* **2005**, *47*, 125; b) A. P. V Soares, M. F. Portela, A. Kiennemann, L. Hilaire, J. M. M. Millet, *Appl. Catal. A Gen.* **2001**, *206*, 221; c) E. Söderhjelm, M. P. House, N. Cruise, J. Holmberg, M. Bowker, J.-O. Bovin, A. Andersson, *Top. Catal.* **2008**, *50*, 145; d) M. R. Sun-Kou, S. Mendioroz, J. L. G. Fierro, J. M. Palacios, A. Guerrero-Ruiz, *J. Mater. Sci.* **1995**, *30*, 496.

[17] a) F. Rafiee, *Curr. Org. Chem.* **2019**, *23*, 390; b) F. Quignard, A. Choplin, A. Domard, *Langmuir* **2000**, *16*, 9106.

[18] a) Q. Wu, L. Wang, B. Zhao, L. Huang, S. Yu, A. J. Ragauskas, *J. Colloid Interface Sci.* **2022**, *605*, 82; b) N. Maslamani, S. B. Khan, E. Y. Danish, E. M. Bakhsh, K. Akhtar, A. M. Asiri, *Chemosphere* **2022**, *291*, 133010; c) K. Hasan, I. A. Shehadi, N. D. Al-Bab, A. Elgamouz, *Catalysts* **2019**, *9*, 839; d) S. Chen, W. Wen, X. Zhao, Z. Zhang, W. Li, Y. Zhang, B. Li, L. Zhu, *Molecules* **2022**, *27*, 7962. e) M. A. Mohd Adnan, B. L. PHoon, N. M. Julkapli, *J. Clean. Prod.* **2020**, *261*, 121190.

RESEARCH ARTICLE

[19] P. F. S. Pereira, A. C. A. de Paula e Silva, B. N. A. da Silva Pimentel, I. M. Pinatti, A. Z. Simões, C. E. Vergani, D. F. Barreto-Vieira, M. A. N. da Silva, M. D. Miranda, M. E. S. Monteiro, A. Tucci, C. Doñate-Buendía, G. Mínguez-Vega, J. Andrés, E. Longo, *Sci. Rep.* **2022**, *12*, 8118.

[20] I. Sorribes, D. Ventura-Espinosa, M. Assis, S. Martín, P. Concepción, J. Bettini, E. Longo, J. A. Mata, J. Andrés, *ACS Sustain. Chem. Eng.* **2021**, 9, 2912.

[21] K. Zheng, F. Yang, Z. Huang, Y. Zhan, Z. Xiao, W. Li, W. Wang, C. Qin, *J. Mater. Res. Technol.* **2022**, *20*, 3905.

[22] M. Assis, A. F. Gouveia, L. K. Ribeiro, M. A. Ponce, M. S. Churio, O. N. Oliveira Jr., L. H. Mascaro, E. Longo, R. Llusar, E. Guillamon, *J. Andres, Appl. Catal. A Gen.* **2023**, *625*, 119038.

[23] P. F. S. Pereira, A. C. A. de Paula e Silva, B. N. A. da Silva Pimentel, I. M. Pinatti, A. Z. Simões, C. E. Vergani, D. F. Barreto-Vieira, M. A. N. da Silva, M. D. Miranda, M. E. S. Monteiro, A. Tucci, C. Doñate-Buendía, G. Mínguez-Vega, J. Andrés, E. Longo, *Sci. Rep.* **2022**, *12*, 8118.

[24] T. S. Freitas, F. S. Oliveira, R. P. Cruz, R. L. S. Pereira, A. R. P. Silva, J. V. B. Moura, C. Luz-Lima, B. C. Viana, J. H. da Silva, P. T. C. Freire, H. D. M. Coutinho, *Eur. J. Pharm. Sci.* **2018**, *123*, 295.

[25] C. Bangyekan, D. Aht-Ong, K. Srikulkit, *Carbohydr. Polym.* **2006**, *63*, 61.

[26] Z. Y. Li, W. B. Song, E. J. Liang, *J. Phys. Chem. C* **2011**, *115*, 17806.

[27] J. V. B. Moura, G. S. Pinheiro, P. T. C. Freire, J. M. Filho, G. D. Saraiva, B. C. Viana, C. Luz-Lima, *Vib. Spectrosc.* **2016**, *87*, 88.

[28] K. Routray, W. Zhou, C. J. Kiely, W. Grünert, I. E. Wachs, *J. Catal.* **2010**, *275*, 84.

[29] Ü. Kersen, R. L. Keiski, *Catal. Commun.* **2009**, *10*, 1039.

[30] M. Fernandes Queiroz, K. R. Melo, D. A. Sabry, G. L. Sassaki, H. A. Rocha, *Mar. Drugs* **2015**, *13*, 141.

[31] C. Song, H. Yu, M. Zhang, Y. Yang, G. Zhang, Int. J. *Biol. Macromol.* **2013**, *60*, 347.

[32] M. Fernandes Queiroz, K. R. Melo, D. A. Sabry, G. L. Sassaki, H. A. Rocha, *Mar. Drugs* **2015**, *13*, 141.

[33] S.-H. Lim, S. M. Hudson, *Carbohydr. Res.* **2004**, *339*, 313.

[34] M. Fernandes Queiroz, K. R. Melo, D. A. Sabry, G. L. Sassaki, H. A. Rocha, *Mar. Drugs* **2015**, *13*, 141.

[35] G. Lawrie, I. Keen, B. Drew, A. Chandler-Temple, L. Rintoul, P. Fredericks, L. Grøndahl, *Biomacromolecules* **2007**, *8*, 2533.

[36] a) R. S. Vieira, M. L. M. Oliveira, E. Guibal, E. Rodríguez-Castellón, M. M. Beppu, *Colloids Surf. A Physicochem. Eng. Asp.* **2011**, *374*, 108; b) G. Lawrie, I. Keen, B. Drew, A. Chandler-Temple, L. Rintoul, P. Fredericks, L. Grøndahl, *Biomacromolecules* **2007**, *8*, 2533.

[37] G. Lawrie, I. Keen, B. Drew, A. Chandler-Temple, L. Rintoul, P. Fredericks, L. Grøndahl, *Biomacromolecules* **2007**, *8*, 2533.

[38] A. I. Cervantes-Macías, C. A. Huerta-Aguilar, T. Pandiyan, *J. Clust. Sci.* **2017**, *28*, 1897.

[39] M. M. Hassan, *Int. J. Biol. Macromol.* **2018**, *118*, 1685.

[40] a) S. Hussain, Y. Wang, L. Guo, T. He, *J. Photochem. Photobiol. C Photochem. Rev.* **2022**, *52*, 100538; b)   H. Wang, X. Li, X. Zhao, C. Li, X. Song, P. Zhang, P. Huo, X. Li, *Chinese J. Catal.* **2022**, *43*, 178.

[41] a) O. Shtyka, R. Ciesielski, A. Kedziora, S. Dubkov, D. Gromov, M. Zakrzewski, T. Maniecki, *Appl. Catal. A Gen.* **2022**, *635*, 118541; b) N. Serpone, A. V Emeline, *J. Phys. Chem. Lett.* **2012**, *3*, 673; c) M Ryzhii, V Ryzhii, R Suris, C Hamaguchi, *Semicond. Sci. Technol.* **2001**, *16*, 202.

[42] a) M. Assis, F. C. Groppo Filho, D. S. Pimentel, T. Robeldo, A. F. Gouveia, T. F. D. Castro, H. C. S. Fukushima, C. C. de Foggi, J. P. C. da Costa, R. C. Borra, J. Andrés, E. Longo, *ChemistrySelect* **2020**, *5*, 4655; b) M. Assis, C. C. de Foggi, V. Teodoro, J. P. de Campos da Costa, C. E. Silva, T. Robeldo, P. F. Caperucci, C. E. Vergani, R. C. Borra, I. Sorribes, A. F. Gouveia, M. A. San-Miguel, J. Andrés, E. Longo, *Appl. Surf. Sci.* **2021**, *545*, 148964.

[43] S. Siahrostami, G.-L. Li, V. Viswanathan, J. K. Nørskov, *J. Phys. Chem. Lett.* **2017**, *8*, 1157.

[44] M. Assis, J. S. da Silva, M. O. Gonçalves, J. M. de Almeida Rodolpho, B. D. de Lima Fragelli, A. B. P. Corte, L. K. Ribeiro, M. D. Teodoro, F. de Freitas Anibal, C. P. de Sousa, O. N. Oliveira, J. Andrés, E. Longo, *Biomater. Adv.* **2022**, *141*, 213097.

[45] A. E. B. Lima, R. Y. N. Reis, L. S. Ribeiro, L. K. Ribeiro, M. Assis, R. S. Santos, C. H. M. Fernandes, L. S. Cavalcante, E. Longo, J. A. O. Osajima, G. E. Luz, *J. Alloys Compd.* **2021**, *863*, 158731; b) A. C. M. Tello, M. Assis, R. Menasce, A. F. Gouveia, V. Teodoro, N. Jacomaci, M. A. Zaghete, J. Andrés, G. E. Marques, M. D. Teodoro, A. B. F. da Silva, J. Bettini, E. Longo, *Inorg. Chem.* **2020**, *59*, 7453; c) M. J. S. Chaves, G. O. Lima, M. Assis, C. J. S. Mendonça, I. M. Pinatti, A. F. Gouveia, I. L. Viana Rosa, E. Longo, M. A. P. Almeida, T. C. R. S. Franco, *J. Solid State Chem.* **2019**, *274*, 270; d) S. C. S. Lemos, T. K. de L. Rezende, M. Assis, F. da C. Romeiro, D. A. Peixoto, E. de O. Gomes, G. M. Jacobsen, M. D. Teodoro, L. Gracia, J. L. Ferrari, E. Longo, J. Andrés, R. C. de Lima, *Mater. Res. Bull.* **2022**, *152*, 111849; e) C. Yin, T. Ye, Y. Yu, W. Li, Q. Ren, *Microchem. J.* **2019**, *144*, 369.

[46] B. Yuan, J. Wu, N. Qin, E. Lin, Z. Kang, D. Bao, *Appl. Mater. Today* **2019**, *17*, 183.

[47] Z. Chen, K. Xia, X. She, Z. Mo, S. Zhao, J. Yi, Y. Xu, H. Chen, H. Xu, H. Li, *Appl. Surf. Sci.* **2018**, *447*, 732.

[48] G. Louit, S. Foley, J. Cabillic, H. Coffigny, F. Taran, A. Valleix, J. P. Renault, S. Pin, *Radiat. Phys. Chem.* **2005**, *72*, 119.

[49] H. F. V Victória, D. C. Ferreira, J. B. G. Filho, D. C. S. Martins, M. V. B. Pinheiro, G. de A. M. Sáfar, K. Krambrock, *Free Radic. Biol. Med.* **2022**, *180*, 143.

[50] A. Gomes, E. Fernandes, J. L. F. C. Lima, *J. Biochem. Biophys. Methods* **2005**, *65*, 45.

[51] D. Meyerstein, *Nat. Rev. Chem.* **2021**, *5*, 595.

[52] a) C. Shen, H. Chen, S. Wu, Y. Wen, L. Li, Z. Jiang, M. Li, W. Liu, *J. Hazard. Mater.* **2013**, *244–245*, 689; b)   M. Z. A. Yahya, A. K. Arof, *Eur. Polym. J.* **2002**, *38*, 1191.

RESEARCH ARTICLE

Entry for the Table of Contents
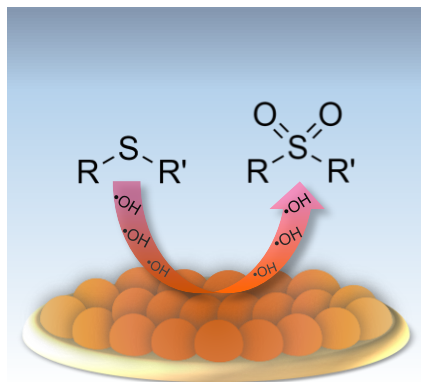
Oxidation of sulfide to sulfone is an important process in organic chemistry, considering the role of sulfone in fine chemical industry and biological compounds. Therefore, green oxidation and a selective catalyst is desirable. On that matter, $Fe_2(MoO_4)_3$ immobilized I chitosan films was synthesized and applied on a group of sulfides, resulting in higher conversion to sulfone and great recyclability.

Institute and/or researcher Twitter usernames: @_mar_telo, @larakribeiro, @UJIuniversitat, @CDMF_comunica